Parametric modeling of components for selection and specification of hybrid vehicle drivetrains

PARAMETRIC MODELING OF COMPONENTS FOR SELECTION AND SPECIFICATION OF HYBRID VEHICLE DRIVETRAINS

THEO HOFMAN, MAARTEN STEINBUCH
Technische Universiteit Eindhoven,
P.O. Box 513, 5600 MB EINDHOVEN, The Netherlands,
Phone: +31 40 247 2798, Fax: +31 04 246 1418, E-mail: T.Hofman@tue.nl

ROËLL VAN DRUTEN, ALEX SERRARENS
Drivetrain Innovations BV,
Horsten 1, 5612 AX EINDHOVEN, The Netherlands,
Phone: +31 40 247 4189, Fax: +31 40 247 5904

Abstract

Drivetrain hybridization implies adding a Secondary power source to a Primary power source in order to improve a multiple of driving functions: Fuel economy, Emissions, Driveability, Comfort and Safety. Designing a hybrid vehicle drivetrain fulfilling the required vehicle driving functions is therefore a complex task. Many researchers have put effort formulating and developing of overall hybrid drivetrain analysis, design and optimization models including top-level vehicle control strategy. This paper seeks to investigate the possibility of overall model simplification for the hybrid drivetrain system including the control strategy by describing the component efficiencies and control rules with only a total amount of 8 characteristic parameters that capture the essence of the system (regarding fuel economy and emissions) with sufficient accuracy (~4%). In contrary to the relative large amount of required static efficiency data and different control rules used in the Simulink/Advisor platform and the relative long computation time with Dynamic Programming. The method has been demonstrated on a series -, a parallel - and a series-parallel hybrid drivetrain with specified component technologies and control strategies.

Keywords: Hybrid Electric Vehicles, System Design Optimization, Modeling and Simulation, Hybrid Strategy, Energy Efficiency, Energy Consumption, Power train, Transmission, Optimal control.

1 Introduction

Ongoing emission legislation and increasing fuel prices pursue many leading vehicle manufactures, and their suppliers to put effort in developing and manufacturing new efficient though cost-effective drivetrain technologies. On nowadays passenger vehicle market, hybrid vehicles are readily available, e.g., the Honda Civic IMA, Toyota Prius, Ford Escape, and the Lexus RX400h. All these vehicles fulfill almost the same hybrid functions, e.g., energy recuperation during braking, motor-assisting, engine off during standstill. However, their drivetrain topology, technology, and control are completely different. The objectives of a hybrid drivetrain are to improve the driving functions of a vehicle: Fuel economy, Emissions, Driveability, Comfort, and Safety. Drivetrain hybridization implies adding a Secondary power source (S) to a Primary power source (P) in order to improve the driving functions. Hybridization allows performing Brake Energy Recuperation (BER), downsizing of the engine, and optimizing the power flows over the different thermal, mechanical, and electrical paths between the different power sources and sinks. Due to the complexity of hybrid vehicle drivetrains, the design of topologies, component technologies, and the control strategy forms a considerable challenge for engineers. Therefore, many researchers have devoted their attention to develop different hybrid drivetrain evaluation, and design tools [1-6]. Most of the design tools are based on the determination of the optimal component sizing, parameters and corresponding supervisory control algorithm for the system components by minimization of fuel economy along a trajectory, and other vehicle performance constraints (e.g. US government performance criteria). These optimizations are

usually based on pre-defined drivetrain topologies, specific component technologies and control strategies. In [4] and [5], a high level-design space framework is discussed, which forms the basis of the development of a more flexible drivetrain modeling, and optimization design tool. Some of the described approaches [6], [7] use ADVISOR [2] as vehicle simulation platform. Instead, research is then focused on developing system design optimization tools. Since, the overall performance of the vehicle is determined by optimal control of the subsystems to its best performance, other approaches use globally optimal control strategy based on Dynamic Programming (DP) in combination with optimal component sizing, and vehicle design parameters [8].
However, an integral design approach is usually characterized by large computational times, complex design problem (optimization) formulations, multiple subsystem simulations, analyses, and non-smooth or non-continuous models. In addition, insights into the design problem at hand are lost when a single final design proposal is presented as a result of a complex integral design process. Interactions between the different drivetrain components, topology and control are then difficult to investigate. This paper forms a contribution in substantially alleviating the complex design problem of hybrid vehicle drivetrains. It does this by abstracting the hybrid drivetrain into quasi-static power sources, -sinks and transmissions characterized only by 2-parameter and 3-parameter efficiency models and operational boundaries.

1.1 Contribution and outline of the paper

In literature several modeling methodologies may be found and a broad overview is presented in Chapter 4 *System Modeling* of book [9].This paper presents an iterative design approach in characterizing the component technologies, selecting the topologies and designing the control strategy of hybrid drivetrains. Thereby, the main research questions are:

(i) Can the component efficiencies and the control be described with sufficient accuracy by a limited set of characteristic parameters?
(ii) What is the relationship between the component technology, the topology and the control strategy?

These questions will be solved in this paper and demonstrated using series, parallel and series-parallel topologies. In Figure 1 an overview is given of the iterative modeling process. Since, the used component models are strongly simplified they must be verified and adapted. This is done by comparing the fuel economy, emissions and the control strategy with that of a detailed model until the required accuracy is obtained. Refined models and control strategy are obtained using the simulation platform ADVISOR [2] and DP respectively. Furthermore, the sub-optimal strategies as implemented in ADVISOR based on test data [10] [11] for the Toyota Prius with leading performance parameters can be improved significantly. In this paper, for comparison reasons, the main vehicle parameters and the drive cycle describing the vehicle load are pre-defined. Topology -, component – and control models are discussed in the Sections 2, 3 and 4 respectively (see Figure 1). The simulation results of the topology, component technology and parametric study are discussed in Section 5. Finally, the discussion and conclusions are described in the Section 6 and 7 respectively.

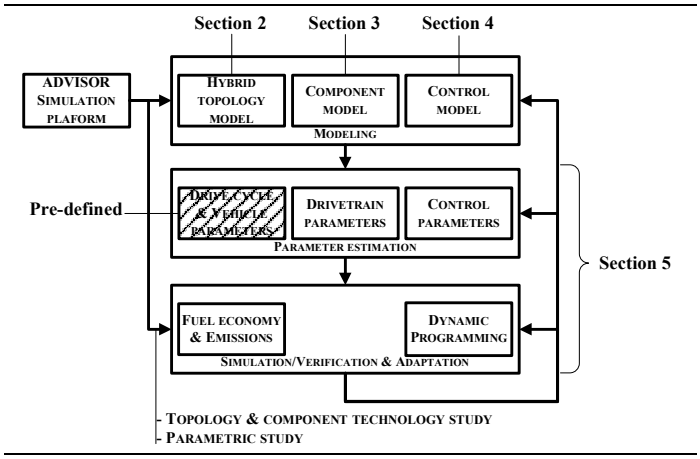

Figure 1: Iterative modeling process.

2 Hybrid topology model

A classification overview of different example transmissions for hybrid drivetrain topologies is shown in the Figure 2. In the Figure 2 also the black box models describing P, S, Transmission technology (T) and the Vehicle wheels (V) are shown. A drivetrain topology defines the possible connections and puts constraints on the transmission ratios between P, S, and V. For the series -, and the series-parallel

transmission the advantage is that S is integrated with T. However, looking at a higher abstraction level for both transmission types S is functionally coupled to the wheel-side of the transmission (Figure 2 (right)). Thereby, the intrinsic functions for S are defined as performing BER and propulsion only by S while P is shut-off eliminating the engine drag – and friction losses. In addition, charging or motor-assisting during driving is possible with S.

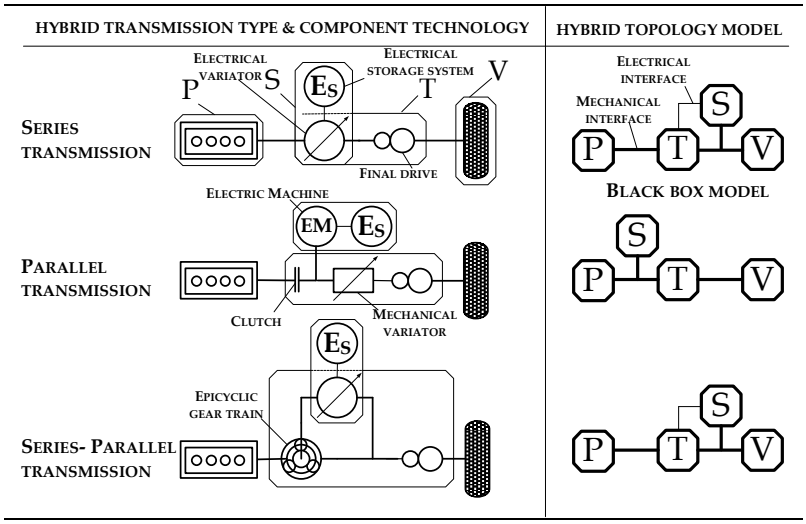

Figure 2: Classification overview of different hybrid technologies and topologies.

However, in case of the series or the series-parallel transmission this can also be done with the electric machine connected at the engine-side. Both electric machines are part of T. For the parallel transmission S is connected at the engine-side of T. For vehicle handling and comfort reasons the largest amount of braking power is supplied by the front-wheel brakes. Usually, S is connected to the front-wheels, thereby maximizing the BER efficiency. The variator of the series -, and the parallel transmission consists respectively of two electric machines, and a push-belt Continuously Variable Transmission (CVT). One of the major advantages of the series transmission is the infinitely variable transmission ratio. Thereby, it is possible to operate the engine and the generator intermediately, but continuously at its highest efficiency point(s). However, at higher requested vehicle loads, the transmission losses of the electrical variator are typically larger than compared to a mechanical variator. The CVT losses in the parallel transmission are lower at higher vehicle loads, but due to the overdrive constraint not all optimal operating points of the engine can be reached. The series-parallel transmission combines the electrical -, and mechanical paths with its advantages, which consists of a planetary gear set combined with two electric machines, which form the variator part of T. The advantages of a series-parallel transmission, compared to a series transmission are:

- The transmission efficiency is higher, because most of the power is transmitted over the mechanical branch;
- An electrical variator with a lower maximum power specification can be used.

However, a disadvantage is the possible occurrence of re-circulation of power flow thereby reducing the transmission efficiency. The operation of the variator and the influence of the battery power on the power flows, and the overall efficiency are discussed in more detail in [13]. It can be concluded, that a topology and a transmission technology add kinematical constraints which restrict the possible transmission ratios between P, S, and V, that can be obtained.

3 Component model

The control sampling time for the Power-Management Controller (PMC) for hybrid drivetrain systems is ~1 [Hz]. The PMC creates set points for servo-loop control systems, which operate at much higher frequency (~20-100 [Hz]). Moreover, using a sampling interval of 1 [s], dynamic behavior of the components can be neglected allowing their characteristics to be represented by static power-based models, which are efficient in use [14]. The only dynamic equation, which is an integrator, holds for the energy storage system. If an affine relationship is assumed (see Figure 3), then the input power P_{in} [W] as a function of the angular speed ω [rad/s] given the output power P_{out} [W] becomes, $P_{in} = \phi(\omega,P_{out}) \approx c_1(\omega,P_{out})\ P_{out} + c_0(\omega,P_{out})$ with the inverse efficiency ϕ [-], the fixed power losses c_0 [W], and the reciprocal of the inner efficiency c_1 [-].

Furthermore, the variable P_{max} represents the output power limitation of the component. In order to capture the high power-loss effects for some components a second order approximation gives better-fit results [13]. Since, the static losses play an important role in the component efficiency, another advantage of this description is, that it is possible to determine these static losses quite well. In contrary to measuring -, or estimating the efficiency on-line. Since, the efficiency is very sensitive for low input powers and is therefore difficult to determine.

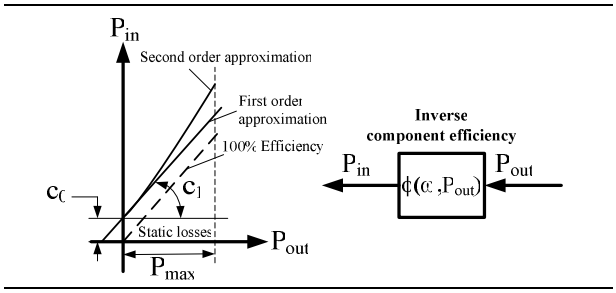

Figure 3: An affine relationship between input and output power and a schematic block representing the inverse component efficiency.

4 Control model – Rule-Based EMS

The control model used in this paper is based on a Rule-Based (RB) Energy Management Strategy (EMS) as is described in [12]. Thereby, the hybrid drivetrain can be operated in certain distinct driving modes. In Figure 4, a block diagram is shown for the power distribution between the different energy sources, i.e., fuel tank with stored energy E_f, S with stored energy E_s, and the vehicle driving over a drive cycle represented by a required energy E_v. The efficiencies of the fuel combustion in the engine, the storage and electric motor S, and the Transmission (T) are described by the variables η_p, η_s, and η_t respectively. The energy exchange between the fuel tank, S and the vehicle can be performed by different driving modes (depicted by the thick lines). The engine power at the crankshaft is represented by P_p. The power demand at the wheels (P_v), and the power flow to and from S (P_s) determines which driving mode is active. The following operation modes are defined:

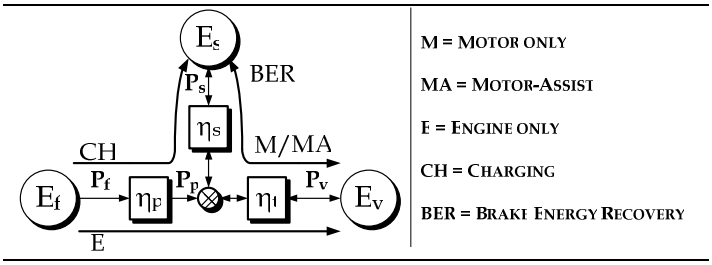

Figure 4: Power flows for different hybrid driving modes. S is connected at the engine-side.

- M: Motor only mode, the vehicle is propelled only by the electric motor and the battery storage supply S up to a certain power level $P^*_{s,max}$, which is not necessary equal to the maximum power $P_{s,max}$. The engine is off, and has no drag -, and idle losses.
- BER: Brake Energy Recovery mode, the brake energy is recuperated up to the maximum generative power limitation $P_{s,min}$, and stored into the accumulator of S. The engine is off, and has no drag -, and idle losses.
- CH: Charging mode, the instantaneous engine power is higher than the power needed for driving. The redundant energy is stored into the accumulator of S.
- MA: Motor-Assisting mode, the engine power is lower than the power needed for driving. The engine power is augmented by power from S.
- E: Engine only mode, only the engine power is used for propulsion of the vehicle. S is off, and generates no losses.

During the M, and the BER mode the engine is off, and as a consequence uses no fuel. This is also referred to as the Idle-Stop (IS) mode. In order to fulfill the integral energy balance constraint over the drive cycle, the energy required for the M and the MA mode needs to be regenerated during the BER mode, or charged during the CH mode. To explain the basic principles of the RB EMS, which is a trade-off between energy balance, and fuel consumption, consider the following two cases, with two different $P_{s,min}$ whereby the energy recuperated during the BER mode for supplying the energy during the M mode over a complete drive cycle is: (i) not sufficient, and (ii) more than sufficient.

(I) The additional required energy for the M mode has to be charged during the CH mode resulting in additional fuel cost.

(II) The redundant energy of the BER mode can be used for motor-assisting during the MA mode resulting in additional fuel savings.

Both cases are schematically shown in the Figure 5. Referring to case I, if $P^*_{s,max}$ is lowered, then the additional fuel cost becomes lower due to decrease of the required charging energy. However, the fuel saving due to the M mode is also reduced, and vice-versa, if $P^*_{s,max}$ is increased. The same holds for case II: The fuel saving during the MA mode is increased if $P^*_{s,max}$ is lowered, but the fuel saving due to the M mode is reduced. For both cases, additional charging during driving and using for motor-assisting can be beneficial, if the energy is charged at a lower driving power, and this energy is used for motor-assisting at a higher driving power. However, the additional fuel saving is relatively small, because the drive energy at higher powers is relatively small. For more details concerning calculation of $P^*_{s,max}$ is referred to [12].

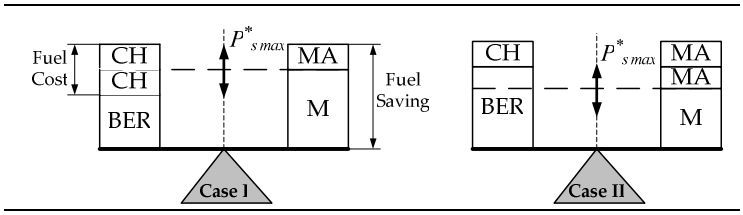

Figure 5 : Energy balance and fuel consumption.

4.1 Energy management optimization problem

The optimization problem is finding the optimal control power flow $P_s(t)$ given a certain power demand at the wheels P_v, while the cumulative fuel energy is minimized subjected to several constraints, i.e.,

$$J(E_s, P_s) = \min_{P_s} \int_o^\tau P_f(E_s, P_s)dt, \quad s.t. \quad \vec{h} = 0, \vec{g} = 0, \tag{4.1}$$

where the fuel power P_f is the product of the fuel rate $\dot{m}_f$ [g/s] and the lower heating value h_{lv} [J/g] for fuel. The main constraints are energy conservation balance of E_s over the drive cycle, constraints on the power P_s, and the energy E_s: $h_1 := \Delta E_s(\tau) = E_s(\tau) - E_s(0) = 0$, $g_{1,2} := P_{s,min} \le P_s(t) \le P_{s,max}$, $g_{3,4} := E_{s,min} \le E_s(t) \le E_{s,max}$. The relative energy change is represented by the variable $\Delta E_s(\tau)$. Using DP the finite horizon optimization problem is translated into a finite computation problem [16]. Note that in principle the technique results in an optimal solution for the EMS, but that the grid step size also influences the accuracy of the result.

4.2 Simulation approach – DP

The operation points in the static-efficiency map of an engine, which maximizes the engine or the system efficiency are collected by the Engine – (EOOL) or the System Optimal Operation Line (SOOL) respectively for a given engine power P_p and secondary power P_s. The transmission efficiency $\eta_t = P_v/P_p$ is determined by the engine torque T^*_p, and speed ω^*_p (pre-scribed by the EOOL/SOOL). However, the required T^*_p, and ω^*_p are determined by $\eta_t = P_v/\phi_t(\omega_t, P_v)$ and the required P_v. Due to this causality conflict it is impossible to determine the T^*_p, and ω^*_p exactly. In this study the losses in T and S are estimated, and are compensated in the following procedure (see Figure 6):

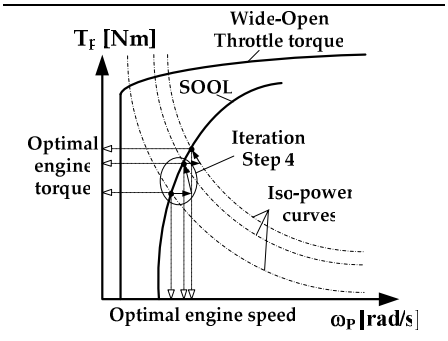

Figure 6: Drivetrain loss compensation procedure.

1. Given the requested P_v, T^*_p, ω^*_p are determined without any drivetrain losses at t = 0. Using these values the modified η_t can be calculated;
2. The difference between P^*_p times the modified η_t, and P_v is used to calculate the modified P^*_p at the initial iteration step;
3. The modified P^*_p is used to calculate the modified T^*_p, and ω^*_p (using the EOOL/SOOL). The modified η_t is calculated by using the modified T^*_p, and ω^*_p at the next iteration step;
4. Steps 2 and 3 are repeated until the power difference between the iteration steps at a certain time step becomes very small;

At later time steps the required P^*_p can be calculated using the known values for the efficiencies at the previous step. Thereto, the requested P_v is divided by the computed η_t. Using the modified T^*_p, and ω^*_p

pre-scribed by the EOOL or the SOOL, which are stored-in look-up tables, the optimal power flow out P_s is calculated using DP given the drive cycle and the vehicle parameters.

4.3 Reference control models - ADVISOR

For comparison the control strategies as are implemented in ADVISOR [2] are compared with the results from the RB EMS and DP. In the Table 1 the rule-based conditions that define which hybrid mode is active for the different hybrid transmission types are given, which will discussed the Section 4.3.1 in more detail. Thereby, the battery is allowed to operate within a certain defined State-Of-Charge (*SOC)* window, i.e., $SOC \in [SOC_{low}, SOC_{high}]$. The control parameters as implemented in ADVISOR were optimized to achieve the highest fuel economy while the final *SOC* is maintained within a certain zero change in *SOC* +/- 0.5% tolerance band.

Table 1: Rule-based control models as are implemented in ADVISOR

Mode:	Rule-based condition:
BER	$SOC < SOC_{high} \cap T_v < 0$
M	$SOC \geq SOC_{low} \cap \{P_p < f_{0,1}\, P_{p,max} \cup [T_p < f_{1,1}\, T_{p,max}(\omega_p) \cup v < v_0\,(SOC)]^* \cup [v < v_0]^{**}\}$
CH	$SOC < SOC_{low} \cup SOC < SOC_{ref} \cap \{\, f_{0,1}\, P_{p,max} \leq P_p \leq f_{0,2}\, P_{p,max}\}$
E	$SOC = SOC_{ref} \cap \{f_{0,1}\, P_{p,max} \leq P_p \leq f_{0,2}\, P_{p,max}\}$
MA	$SOC \geq SOC_{low} \cap \{P_p > f_{0,2}\, P_{p,max} \cup [T_p > T_{p,max}(\omega_p)]^{*,**}\}$

Additionally, in case of the *parallel transmission with CVT or the **series-parallel transmission

4.3.1 Hybrid modes and the control parameters

Two power fraction parameters $f_{0,1}$ and $f_{0,2}$ of the maximum available engine power $P_{p,max}$ respectively determine the minimum and the maximum operation power level of the engine, which are focused on eliminating the relative low efficiency areas of the engine. If the *SOC* gets too low, then the battery is charged during driving (CH mode) with a certain charging power P_{ch} which is a linear function of the *SOC* and is zero when the *SOC* is equal to the average value of the maximum and the minimum *SOC* which is default the reference *SOC* or SOC_{ref}. Except for the parallel transmission a ratio of the charge torque and the maximum engine torque is compared with the pre-defined engine torque fraction $f_{2,1}$ of the maximum engine torque at a certain speed $T_{p,max}(\omega_p)$ that the engine will operate at when lower torque fractions are requested. Then, for charging the maximum torque T_{ch} of both possibilities is chosen, i.e., $T_{ch} = \max(P_{ch}/\omega_p, f_{2,1} \cdot T_{p,max}(\omega_p))$. Furthermore, if the $SOC \geq SOC_{low}$, then a pre-selected value for the fraction of the maximum engine torque $f_{1,1}$ at each speed at which the engine should turn off is compared with current ratio of the requested engine torque and the maximum engine torque for a certain requested engine speed. Within control strategies for the parallel and the series-parallel transmission it is possible to select the vehicle electric launch speed threshold v_0, below this threshold the engine is also turned off. However, for the parallel transmission v_0 is a linear function of the *SOC*, which is minimum and maximum at SOC_{low} and SOC_{high} respectively. Furthermore, with the series transmission if the electric machine at the wheel side (generator) is not able to supply the required driving power then the engine and the generator (genset) are turned on. When the genset is on, the minimum engine power level determines the charging power, which can be larger than the requested electric input power to the motor. Then, the battery is charged as long as requested battery power is larger than the maximum discharging power of the battery. The minimum voltage of the motor or the battery limits the maximum discharging power. If neither of these limits are exceeded then the maximum power observed is equal to open-circuit voltage divided by two. Basically, the same holds for charging, but the maximum charging power is mainly limited by the maximum battery voltage. For the series-parallel transmission two control parameters determine mainly the EMS, namely $f_{0,1}$, and v_0. The other parameters $f_{1,1}$ and $f_{0,2}$ are set to zero. The charging power during the CH mode is the output of a proportional controller of which the input is the difference between the current *SOC* and the SOC_{ref}. Furthermore, the engine and the generator of the series transmission are operated at the SOOL. For the parallel transmission the electric machine and the engine are operated separately at the maximum efficiency points during the BER, M and the E mode (EOOL). During the CH and the MA mode the engine and the electric machine are operated at the SOOL. For the series-parallel transmission the engine is operated at the EOOL alone.

5 Parametric component models

In this section the parametric models for P, S, T and the Control strategy (C) will be discussed. The operation points determine the parameters of the static power-based functions. Since, the engine is operated at the optimal operation points these parameters can be calculated in advance for the engine alone. The parameters for S and T will be determined via simulation with ADVISOR and DP respectively. The fitted component parameters for P, S and T will be used in the RB EMS.

5.1 Parametric engine model

In this paper two engine models are used. For reasons of space the modeling of only one engine will be discussed here in more detail. The energy specific fuel consumption β is a function of the engine speed ω_p and engine torque T_p as is shown in Figure 7 (left). If $P_p = T_p\ \omega_p$ is specified $P_f = \phi_p(\omega_p,P_p)$ becomes a function of ω_p alone, i.e., $P_f = \beta(\omega_p, T_p)P_p h_{lv} = \beta(\omega_p, P_p/\omega_p)\ P_p h_{lv}$. The variable h_{lv} represent the lower heating value for fuel. The EOOL connects the optimal operation points, i.e., ω^*_p and $T^*_p = P_p/\omega^*_p$ fulfilling the condition of minimum fuel power, $\partial\phi_p(\omega_p,P_p)/\partial\omega_p = 0$. In the figure also the operation lines are shown for higher fuel consumption in percentage of the values at the EOOL. The ω^*_p for each given P_p gives solutions in the form of the function curve $P_f = \phi_p(\omega^*_p,P_p)$ as is shown in Figure 7 (right).

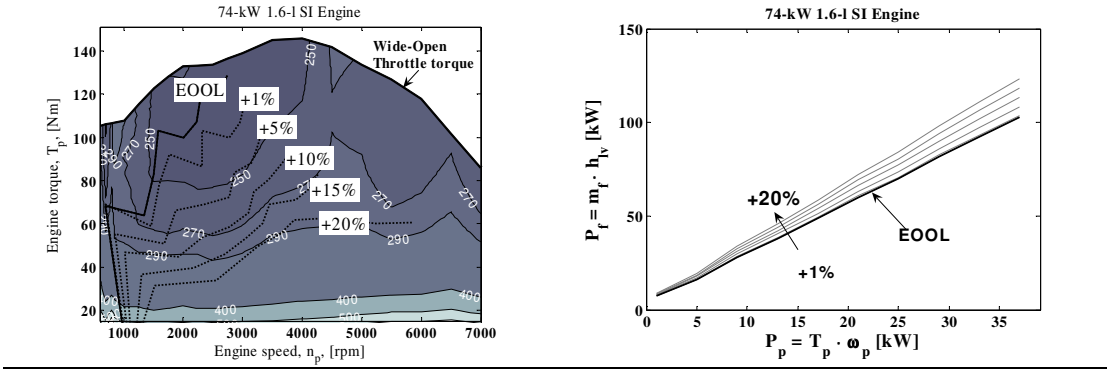

Figure 7: Static efficiency map in energy specific fuel consumption [g/kWh] of a 74-kW 1.6-l SI engine and the fuel input power as a function of the mechanical output power.

5.2 Interaction between the engine parameters, the fuel use and the control strategy

If a first order approximation is used, then the reciprocal of the inner efficiency c_1 and the fixed losses c_0 determine the maximum efficiency and the sensitivity of the efficiency to power respectively. Since, at low power demands the relative contribution of c_0 is larger than at higher power demands. These parameters determine the control strategy. This will be shown with a small example. Assume a constant engine output power demand P_p of 1 [kW] over time period of τ = 15 [s] and with c_1 = 2.5 [-] and c_0 = 3 [kW] describing the engine efficiency. Then, the total required mechanical output energy is 15 [kJ] and the total required fuel energy is $E_{f,1} = \sum^{\tau}_0[c_1 \cdot P_p + c_0]\ \Delta t = \sum^{15}_0[2.5 \cdot 1 + 3]\ 10^3\ \Delta t$ = 82.5 [kJ]. If 2 [kW] was charged during driving into an accumulator in the first time period t_{on} = 5 [s] and re-used for driving with an electric machine allowing the engine to be shut-off over the last time period t_{off} = 10 [s], then the input energy of the engine is significantly reduced to $E_{f,2} = \sum^{\text{ton}}_0[c_1 \cdot P_p\ (1 + (1/\eta^2_s) \cdot (t_{off}/t_{on})) + c_0]\ \Delta t = \sum^{5}_0[2.5 \cdot (1 + 10/5) + 3]\ 10^3\ \Delta t$ = 52.5 [kJ], with the S efficiency represented by the variable η_s Note that the example problem is subjected to the constraint of the energy balance conservation of the accumulator over τ and η_s = 100%. It can be seen that the main fuel energy saving $E_{f,2}$-$E_{f,1}$ = -30 [kJ] of the engine is realized by eliminating the static power losses of 3 [kW] over the last 10 [s]. In addition, it can be shown that the strategy is beneficial, i.e., $E_{f,2} > E_{f,1}$ as long as the efficiency of the electric machine and the accumulator system $\eta_s > \sqrt{}(1/(1+(c_0/c_1)\ P_p))$ = 0.67 [-]. The required η_s is independent on the time periods t_{on} and t_{off}, but dependent on the engine characteristics and the engine power demand. If free energy is recharged during braking, then the efficiency η_s can be lower, while still the above-described strategy is beneficial. Furthermore, the larger the static losses c_0 the larger amount of fuel energy saving can be realized. Usually, an engine

with a smaller displacement has a smaller c_0 due to reduction of the friction and pumping losses. Furthermore as example the Honda IMA does not perform electric driving. Therefore, fuel saving is realized by BER and re-using this energy for motor-assisting, downsizing of the engine, applying idle-stop at stand-still and with use of a Cylinder Idling System (CIS) [15]. The CIS allows reducing the pumping losses (50%) by inactivating the intake and exhaust valves of three cylinders when fuel flow is cut during deceleration.

5.3 Parametric transmission and secondary power source models

In this section the parameters for S, T and C will be discussed. First, the simulation results regarding the fuel economy and emissions with the different simulation methods will be discussed. All simulations performed presented in this paper have been done on the JP10-15 drive cycle. The inertias of the electric machines, engine and auxiliary loads are, for simplicity, assumed to be zero. During braking energy is partially recuperated up to the maximum generative power limitation of the electric machine. In addition, some of the braking energy is dissipated between the front - and the rear-wheels in the wheel-brake discs. The braking energy distribution is pre-scribed by a non-linear function which is dependent on the vehicle speed [2]. During braking the engine is assumed to be shut-off or disengaged eliminating the engine drag losses. The Reference Vehicle (RV) is equipped with a 74-kW 1.6-l SI engine (see Figure 7) and an electronic CVT as is used in the parallel transmission. In Table 5 an overview of the component data is given. The total power specification for every hybrid drivetrain configuration is kept constant at approximately 74 [kW]. In this way the dynamic performance of the vehicle is not compromised.

5.3.1 Simulation results: Fuel economy and emissions

In Table 2 the fuel economy and the emission results for the different hybrid topologies are listed. Although the cost function consists only the fuel consumption, for all hybrid drivetrains the *HC*, *CO* and NO_x emissions are reduced, except regarding the NO_x emissions for the series transmission. This can be solved by using a weighted cost function consisting of the sum of the fuel use and emissions and increasing the weight factor regarding the NO_x emissions. However, this has not been investigated in this paper. The relative influence of downsizing (without a battery) and hybridization (adding an S) on the fuel economy results is shown in Table 3. The largest fuel saving is realized with the series-parallel transmission. Although, the battery and electric machine (30 [kW]) of the parallel transmission are similar to the series-parallel transmission, the overall S efficiency is reduced due to power losses of the CVT. The component efficiencies will be discussed in the Section 5.3.2 in more detail.

Table 2: Simulation results

Test:	Topology:	Fuel economy [l/100km]	Emissions [g/km]†		
			HC	CO	NO_x
Simulink/ADVISOR					
1.	RV / 74 [kW]	8.24	-	-	-
2.	RV / 43 [kW]	6.13	1.53	2.99	0.63
3.	SE	4.99	0.65	2.44	1.10
4.	PA	3.33	0.54	1.62	0.61
5.	SP	2.99	0.49	1.46	0.54
Dynamic Programming					
6.	SE	3.88	0.48	1.64	0.68
7.	PA	3.02	0.48	1.47	0.55
8.	SP	2.84	0.45	1.39	0.53
Rule-Based EMS					
9.	SE	4.04	0.56	1.98	0.85
10.	PA	3.07	0.52	1.49	0.52
11.	SP	2.93	0.49	1.42	0.51

RV: Reference Vehicle; SE: Series; PA: Parallel; SP: Series-Parallel. †at engine exhaust system

Table 3: Fuel economy improvement

	Series ([l/100km])	Parallel	Series-parallel
A: Downsizing	20.9% (6.52)	25.6% (6.13)	28.0% (5.93)
B: Hybridization	36.7% (3.88)	50.7% (3.02)	53.7% (2.84)

A:Reference test 1: 8.24 [l/100km] / B:Reference test 2: 6.13 [l/100km]

5.3.2 Component model parameters

The observed $P^*_{s,max}$ and the fit functions describing the component efficiencies by a few parameters (as listed in Table 4) for P, S and T have been used within the RB EMS in order to calculate the fuel economy and emissions. S is mainly used during the BER/M mode. Therefore, only the affine lines fitted through the operation points in these modes have been used with the RB EMS (see Figure 8 (left)).

Furthermore, due to uncertainty on the found fit coefficients the static losses c_0 for S can be negative. The battery power influences the T efficiency for every transmission topology. In Figure 9, as example, the engine input power as function of the vehicle drive power for different battery powers calculated with DP for the series-parallel transmission is shown. In this paper, for simplicity, the affine lines for T fitted through operation points simulated with a battery power equal to zero over the drive cycle have been used (see Figure 8 (right)). This is allowable, because the implicit sensitivity of the fit coefficients to battery power is small. The difference in fuel consumption due to this assumption is relative small.

Table 4: Estimated model parameters (RB EMS)

		Model parameter		
Component	Topology	c_2 [1/W]	c_1 [-]	c_0 [W]
P (74 [kW])	RV	1.85e-5	2.65	4212
P (43 [kW])	SE/PA/SP	1.16e-5	2.09	5194
S (charging)	SE	-	-0.75	-73
S (discharging)	SE	-	-1.48	-46
T	SE	-	1.40	954
S	PA	-	-0.77	-111
S	PA	-	-1.49	75
T	PA	-	1.11	371
S	SP	-	-0.85	12
S	SP	-	-1.43	43
T	SP	-	1.06	656
Control model	Topology:	SE	PA	SP
C (ADVISOR)	$f_{0,1}$	0.51	0.10	0.12
C (RB EMS)	$P^*_{s,max}$ [W]	8.1	7.0	7.4

6 Discussion

6.1 Control model parameters - ADVISOR

The fuel economy is mainly determined by the control constraints or rules, which determine where the engine is allowed to be turned off (BER/M mode). Therefore, the main control parameters within ADVISOR are $f_{0,1}$, $f_{1,1}$ or v_0 and within the RB EMS is $P^*_{s,max}$ respectively. Other control rules within ADVISOR, which determine the amount of charging - or discharging power during the CH and the MA mode, do have effect on the fuel economy, but the influence is relative small. Since, the efficiency of the engine is then already relative high and the sensitivity of the engine efficiency to power is small. The calibrated $f_{0,1}$ for each transmission is also listed in Table 4. Thereby, $f_{1,1} \geq f_{0,1}$ and v_0 is larger than the maximum cycle speed. The calibrated $f_{0,1}$ for the series transmission is 0.51. At this power fraction the genset is operated at the sweet spot of the engine (lowest β) and energy is charged with minimum fuel cost. However, with DP it was found that the fuel consumption could be reduced if the motor (wheel-side) is partially supplied by the battery up to a battery output power of approximately 7.7 [kW]. At higher power demands the battery power is augmented by power from the engine that is a function of P_v and the *SOC*. It appeared to be not straightforward to adapt the defaults rules within ADVISOR by changing the main control parameters to the preferred optimal control settings. This explains the relative large discrepancy between DP and ADVISOR for the series transmission. Using the results from DP it showed that for the parallel and the series-parallel transmission the optimized $f_{0,1}$ are 0.10 and 0.12 respectively. With the default control parameters as implemented in ADVISOR for series-parallel transmission (Toyota Prius 1998) it was found that in the high-speed areas the engine was not allowed to shut off at relative low P_v resulting in less idle stop. In addition, generative torque of the motor during braking is reduced due to additional engine drag torque. Since, the vehicle speed was then larger than v_0. If v_0 is set to a larger value than the maximum cycle speed effectively more (free) energy is charged during the BER mode than during the CH mode, which reduces the fuel cost. Although, the calibrated $f_{0,1}$ is smaller compared to the default value, which causes that the vehicle is less propelled by the electric machine (wheel-side) during the M mode, the fuel economy is significantly improved due to reduction of the fuel cost during the CH mode. Furthermore, it was found that the optimal EMS is focused on charging during driving in the low-speed areas (<41 [km/h]) by the generator (15 [kW]) and in the high-speed areas by the motor (30 [kW]) respectively.

6.2 Influence of the component efficiencies on the fuel economy

In Figure 11 the energy distribution between different hybrid modes and the relative energy over time for the different topologies and strategies is shown. It can be seen that the energy during BER mode for the series-parallel is larger than for the series and the parallel transmission due to the higher S efficiency during braking. The energy during the M mode for the series transmission is larger than for

the parallel and the series-parallel transmission due to the lower efficiency of the T. Since, the overall S efficiency for the parallel transmission is almost equal to the series transmission.
In the Figure 10 a contour plot of constant fuel use for different $P_{s,max}$ and average constant S efficiencies η_s calculated with the RB EMS for the series-parallel transmission is shown. P and T efficiencies are calculated with the parameters as listed in Table 4. It can be seen that if η_s is decreased at a constant fuel economy, then the power specification $P_{s,max}$ is increased and vice-versa. Although, the electric machine specification is 30 [kW] only 7.4 [kW] is effectively used. The redundant available power is used regarding the dynamic performance. The fuel economy can be improved if η_s is increased, but increasing of $P_{s,max}$ > 7.4 [kW] has overall a negligible effect on the fuel economy. The results of 3.03 [l/km] with η_s = 0.774 is close to test 11. The small difference is caused by the relative small static losses for S. The influence of the other component efficiencies and power specifications (P, T) on the fuel economy can be investigated with this method very easily as well.

7 Conclusions

The fuel economy and emissions for three typical different hybrid drivetrain topologies have been calculated with different simulation models (ADVISOR, DP and RB EMS). The results show that model simplification for the hybrid drivetrain topology, component technologies and control strategy can be done with sufficient accuracy (~4%). Thereby, the component efficiencies and the control model are only described by a total amount of 8 characteristic parameters. In contrary to the relative large amount of required static component efficiency data and different control rules used in ADVISOR and the relative long computation time with DP. Reversibly, if realistic characteristic parameters for P, S and T are determined fulfilling a certain fuel economy and emissions improvement; then component specifications can be derived and consequently the technology and topology can be selected or specified. In this way, control design, optimization, component and topology selection and specification are merged in a single methodology framework.

Table 5: Component data for hybrid drivetrains

Series transmission	
Electric machine (wheel side)	Manufacturer: Westinghouse; 75 [kW] (continuous) AC induction motor/inverter, Torque range: from 271 [Nm] to 72 [Nm] (corresponding speed from 0 [rpm] to 10000 [rpm]). The efficiency map includes the inverter/controller efficiencies.
Electric machine (engine side)	Manufacturer: Mannesmann Sachs; 63 [kW] (continuous) PM motor/inverter, Torque range: from 157 [Nm] to 110 [Nm] (corresponding speed from 0 [rpm] to 5500 [rpm]). The efficiency map includes the inverter/controller efficiencies.
Final drive	The final drive ratio is 0.1472 [-] with a constant efficiency of 0.98 [-]
Parallel transmission	
Electric machine (engine side)	Manufacturer: Toyota; 30 [kW] (continuous) PM motor/inverter, Torque range: from 305 [Nm] to 47.7 [Nm] (corresponding speed from 0 [rpm] to 6000 [rpm]). The efficiency map includes the inverter/controller efficiencies.
CVT/final drive	The electronic CVT has an under-drive and over-drive ratio of 0.5 [-] and 2.5 [-] respectively. The final-drive ratio is 0.1715 [-]. The efficiency map includes the final drive efficiency.
Series-Parallel transmission	
Electric machine (engine side)	Manufacturer: Toyota; 15 [kW] (continuous) PM motor/inverter, Torque range: from 55 [Nm] to 26 [Nm] (corresponding speed from 0 [rpm] to 5500 [rpm]). The efficiency map includes the inverter/controller efficiencies.
Electric machine (wheel side)	Manufacturer: Toyota; 30 [kW] (continuous) PM motor/inverter, Torque range: from 305 [Nm] to 47.7 [Nm] (corresponding speed from 0 [rpm] to 6000 [rpm]). The efficiency map includes the inverter/controller efficiencies.
Planetary gear set/Final drive	The planetary gear set ratio and the final drive ratio are -2.6 [-] and 0.2431 [-] respectively. The efficiencies are both constant 0.98 assumed.
Energy storage system	
Battery pack	Manufacturer: Panasonic; Type: Ni-MH, Nominal voltage 288 [V_{dc}], Capacity 6.5 [Ah] SOC_{low} = 0.30 [-]; SOC_{high} = 0.80 [-]; SOC_{ref} = 0.55 [-];
Vehicle data	
Mass: 1368 [kg], Air drag coefficient: 0.29 [-], Frontal area: 1.746 [m^2], Roll resistance coefficient: 0.9 [%], Maximum regenerative brake fraction: 0.5 [-].	
Engine data	
Manufacturer: Toyota; Displacement and type: 43 [kW] (at 4000 [rpm]) 1.5 [l] SI Atkinson internal combustion engine. Maximum torque: 102 [Nm] at 4000 [rpm]	

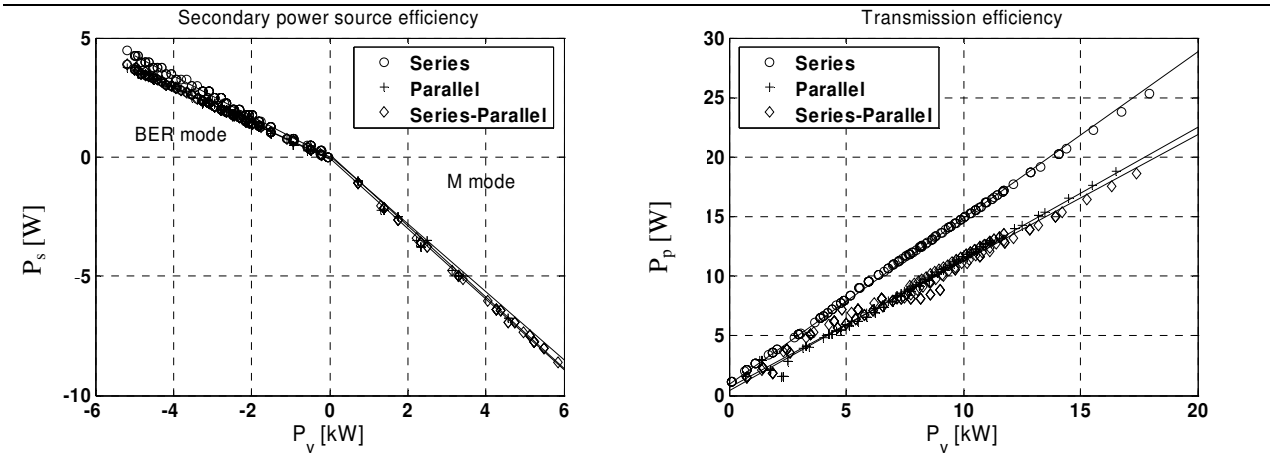

Figure 8: Output power as a function of the input power for S and T.

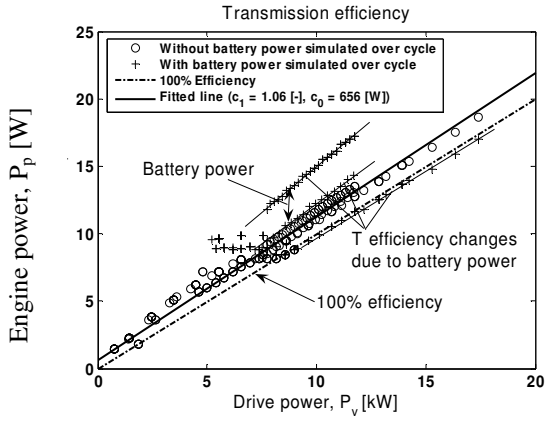

Figure 9: Influence of battery power on transmission efficiency.

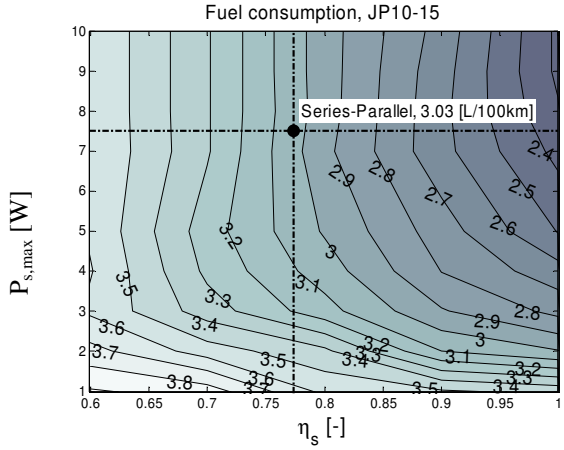

Figure 10: Influence of component specifications for S on the fuel economy.

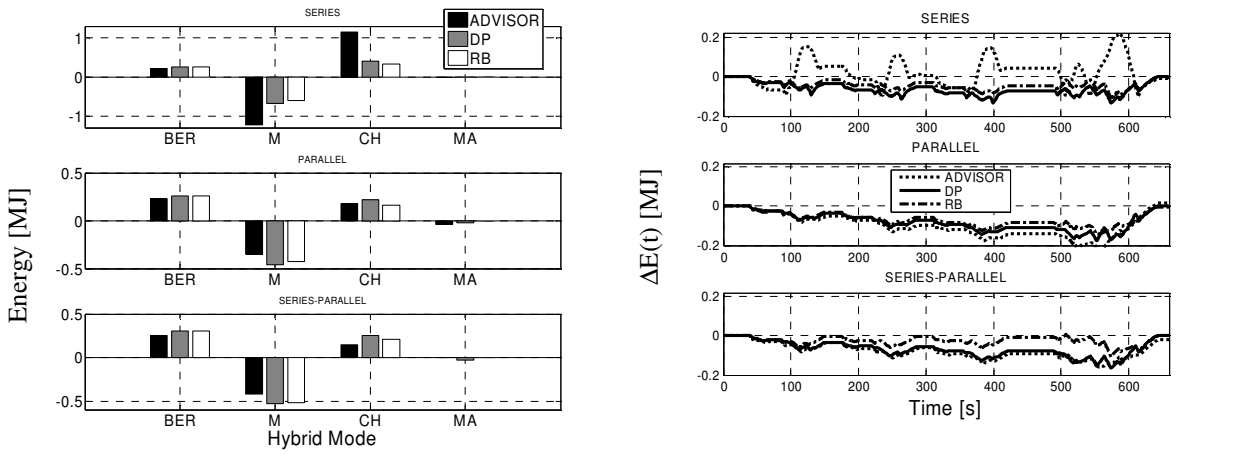

Figure 11: Energy distribution over the hybrid modes and the relative energy over time.

References

[1] Powell, B. K., Bailey, K. E., and Cikanek, , S. R., *Dynamic Modeling and Control of Hybrid Electric Vehicle Powertrain Systems*, In: J. of IEEE-Control Syst. Mag., **18**(5), p.17-33, 1998.

[2] Wipke, K. B., Cuddy, M. R., and Burch S. D., *ADVISOR 2.1: A User-Friendly Advanced Powertrain Simulation Using a Combined Backward/Forward Approach*, In: J. of IEEE-Trans. on Vehicular Technology, **48**, p.1751-1761, 1999.

[3] Butler, K. L., Ehsani, M., and Kamath, P., *A Matlab-Based Modeling and Simulation Package for Electric and Hybrid Electric Vehicle Design*, In: J. of IEEE-Trans. on Vehicular Technology, **48**, p.1770--1778, 1999.

[4] G. Rizzoni, L. Guzzella, and B. M. Baumann, *Unified Modeling of Hybrid Electric Vehicle Drivetrains*, J. of Transactions on Mechatronics, **4**(3), p.246-257, 1999.

[5] L. Guzzella, and A. Amstutz, *CAE Tools for Quasi-Static Modeling and Optimization of Hybrid Powertrains*, In: J. of Transactions on Vehicular Technology, **48**(6), p.1762-1769, 1999.

[6] H.M. Kim, M. Kokkolaras, L.S. Louca, G.J. Delagrammatikas, N.F. Michelena, Z.S. Filipi, P.Y. Papalambros, J.L. Stein, and D.N. Assanis, *Target cascading in vehicle redesign: a class VI truck study*, In: J. of of Vehicle Design, **29**(3), p.199-225, 2002.

[7] A. Molyneaux, G. Leyland, and D. Favrat, *Multi-objective optimisation of vehicle drivetrains*, In: Proc. of Swiss Transport Research Conference, Monte Verita, Ascona, 2003.

[8] Scordia J., Desbois Renaudin M., Trigui R., Jeanneret B., Badin F. *Global optimization of energy management laws in hybrid vehicles using graph theory (submitted)*. In: Int. J. of Vehicle Design. ISSN 0143-3369, 2005

[9] T. Samad, *Perspective in control engineering: technologies, applications, and new directions*, IEEE Press, 2001

[10] K.J. Kelly, M. Mihalic, and M. Zolot, *Battery usage and thermal performance of the Toyota Prius and Honda Insight for various chassis dynamometer test procedures*, In: NREL/CP-540-31306, p.1-6, 2001.

[11] K.J. Kelly, and A. Rajagoplan, *Benchmarking of OEM Hybrid Electric Vehicles at NREL*, In: NREL/TP-540-31386, p.1-101, 2001.

[12] T. Hofman, M. Steinbuch, A. Serrarens, and R. van Druten, *Rule-based energy management strategies for hybrid vehicle drivetrains: A fundamental approach in reducing computation time*, In: Proc. of 4th IFAC-Symposium on Mechatronic Systems, Heidelberg, Germany, 2006.

[13] T. Hofman, M. Steinbuch, and R. van Druten, *Modeling for simulation of hybrid drivetrain components*, In: Proc. of IEEE-Symposium on Vehicular Propulsion and Power, London, UK, 2006.

[14] B. de Jager, *Predictive storage control for a class of power conversion systems*, In: Proc. of the Europ. Control Conf., Cambridge, UK, 2003.

[15] M. Matsuki, Y. Hirano, and A. Matsubara, *Development of a Power Train for the Hybrid Automobile – the Civic IMA*, Honda R&D Technical Paper, EVS21, Monaco, 2005.

[16] R.E. Bellman, *Dynamic programming*, Princeton University Press, 1962.

Author

Theo Hofman was born on the September 5th, 1976 in Utrecht, the Netherlands. He studied Mech. Eng. at the Technische Universiteit Eindhoven (TU/e). Since August 2003, he is a Ph.D. candidate with the Control Systems Technology group. The research programme, named 'Impulse Drive' focuses on the design methodologies for a hybrid vehicle drivetrain with significant reduction of fuel consumption and emissions. TU/e; Dept. of Mech. Eng. (WH –1.127); Section Control Systems Technology; PO Box 513; 5600 MB Eindhoven; The Netherlands. Tel: +31 40 247 2789; Fax: +31 40 246 1418; E-mail: t. hofman@tue.nl.

Roell van Druten finished his Masters in June 1996 and his Ph.D. in October 2001, both at the Technische Universiteit Eindhoven. Currently he is a CEO of Drivetrain Innovations (DTI), which is a licensing and contract-research center on automotive powertrains, transmissions and components. *1) Drivetrain Innovations*: MMP 1.42; Horsten 1; 5612 AX Eindhoven; The Netherlands. Tel +31 40 247 5812; Fax: +31 40 247 5904; E-mail: druten@dtinnovations.nl; URL: www.dtinnovations.nl. *2)* TU/e; *Dept. of Mech. Eng.* (WH -1.125); Section Control Systems Technology; Technische Universiteit Eindhoven; PO Box 513, 5600 MB Eindhoven, The Netherlands, Tel: +31 40 247 4828; Fax: +31 40 246 1418; E-mail: r.m.v.druten@tue.nl;

Alex Serrarens was born 6 september 1973 in Hulst, The Netherlands. He received his MSc-degree MechEng in april 1997 at the Technische Universiteit Eindhoven. In 2001 he received his PhD degree from the same university in the field of powertrain control of passenger cars with CVT. Currently he is business partner within Drivetrain Innovations (DTI) which is a licensing and contract-research center on automotive powertrains, transmissions and components. *Drivetrain Innovations*: MMP 1.42, Horsten 1, 5612 AX Eindhoven , The Netherlands. Tel +31 40 247 5812; Fax: +31 40 247 5904; E-mail: serrarens@dtinnovations.nl.

(S'83-M'89-SM'02) received the M.Sc. degree (cum laude) in mechanical engineering and the Ph.D. degree in modeling and control of wind energy conversion systems from Delft University of Technology, The Netherlands, in 1984 and 1989, respectively. He is currently a Full Professor with the Department of Mechanical Engineering, Technische Universiteit Eindhoven, Eindhoven, The Netherlands. From 1984 to 1987 he was a Research Assistant with Delft University of Technology and KEMA (Power Industry Research Institute), Arnhem, The Netherlands. From 1987 to 1998, he was with Philips Research Laboratories, Eindhoven, as a Member of the Scientific Staff, working on modeling and control of mechatronics applications. From 1998 to 1999, he was a Manager of the Dynamics and Control Group at Philips Center for Manufacturing Technology. His research interests are modeling and control of motion systems. Dr. Steinbuch was an Associate Editor of the IEEE Transaction On Control Systems Technology from 1993 to 1997, of IFAC Control Engineering Practice from 1994 to 1996, and of IEEE Control Systems Magazine from 1999 to 2002. He is currently Editor-at-Large of the European Journal of Control. In 2003, he received the `Best-Teacher 2002/2003' award of the Department of Mechanical Engineering, Technische Universiteit Eindhoven. E-mail: m.steinbuch@tue.nl.